750476

ANL/CHM/CP-99428

THE INFLUENCE OF DESULFOVIBRIO DESULFURICANS ON NEPTUNIUM CHEMISTRY

L. SODERHOLM*, C.W. WILLIAMS*, MARK.R. ANTONIO*, MONICA LEE TISCHLER** AND MICHAEL MARKOS**
*Chemistry Division, Argonne National Laboratory, Argonne, IL, 60439.
ls@anl.gov, mantonio@anl.gov
**Department of Biological Sciences, Benedictine University, Lisle IL

Abstract paper No. R14.3

Presented at the

1999 Fall Materials Research Society Meeting
29 November - 3 December
Boston MA

RECEIVED
JAN 18 2000
OSTI

The submitted manuscript has been created by the University of Chicago as Operator of Argonne National Laboratory ("Argonne") under Contract No. W-31-109-ENG-38 with the U.S. Department of Energy. The U.S. Government retains for itself, and others acting on its behalf, a paid-up, nonexclusive, irrevocable worldwide license in said article to reproduce, prepare derivative works, distribute copies to the public, and perform publicly and display publicly, by or on behalf of the Government.

DISCLAIMER

This report was prepared as an account of work sponsored by an agency of the United States Government. Neither the United States Government nor any agency thereof, nor any of their employees, make any warranty, express or implied, or assumes any legal liability or responsibility for the accuracy, completeness, or usefulness of any information, apparatus, product, or process disclosed, or represents that its use would not infringe privately owned rights. Reference herein to any specific commercial product, process, or service by trade name, trademark, manufacturer, or otherwise does not necessarily constitute or imply its endorsement, recommendation, or favoring by the United States Government or any agency thereof. The views and opinions of authors expressed herein do not necessarily state or reflect those of the United States Government or any agency thereof.

DISCLAIMER

Portions of this document may be illegible in electronic image products. Images are produced from the best available original document.

TEM CHARACTERIZATION OF CORROSION PRODUCTS FORMED ON A STAINLESS STEEL-ZIRCONIUM ALLOY

J.S. Luo* and D.P. Abraham
Chemical Technology Division, Argonne National Laboratory, Argonne, IL 60439
*E-mail address: Luo@cmt.anl.gov

ABSTRACT

The corrosion products formed on a stainless steel-15Zr (SS-15Zr) alloy have been characterized by transmission electron microscopy (TEM) and energy dispersive x-ray spectroscopy (EDS). Examination of alloy particles that were immersed in 90°C deionized water for two years revealed that different corrosion products were formed on the stainless steel and intermetallic phases. Two corrosion products were identified on an austenite particle: trevorite ($NiFe_2O_4$) in the layer close to the metal and maghemite (Fe_2O_3) in the outer layer. The corrosion layer formed on the intermetallic was uniform, adherent, and amorphous. The EDS analysis indicated that the layer was enriched in zirconium when compared with the intermetallic composition. High-resolution TEM images of the intermetallic-corrosion layer interface show an interlocking metal-oxide interface which may explain the relatively strong adherence of the corrosion layer to the intermetallic surface. These results will be used to evaluate corrosion mechanisms and predict long-term corrosion behavior of the alloy waste form.

INTRODUCTION

Stainless steel-zirconium (SS-Zr) alloys have been developed as waste forms to immobilize and retain fission products separated during the electrometallurgical treatment of spent nuclear fuel [1, 2]. The baseline waste form is a stainless steel-15 wt% zirconium (SS-15Zr) alloy, which is prepared by melting appropriate amounts of Type 316 stainless steel (SS316) and high-purity zirconium. The SS-15Zr alloy displays a eutectic microstructure that contains the stainless steel-type phases, ferrite and austenite, and $ZrFe_2$-type Laves intermetallic polytypes C36 (dihexagonal, $MgNi_2$-type) and C15 (cubic, $MgCu_2$-type) [3]. Many fission products, such as Nb, Pd, Rh and Ru, are preferentially incorporated into the $ZrFe_2$–type intermetallics, whereas others such as Tc and Mo are present in all phases of the alloy waste forms [2]. The actinide elements do not form separate actinide-rich phases, but appear as locally enriched regions within the $ZrFe_2$–type intermetallics [2].

A series of tests is being conducted at Argonne National Laboratory to evaluate the corrosion behavior of the SS-15Zr metal waste form. In this paper, we present preliminary results from the microstructural characterization of corrosion layers formed on SS-15Zr alloy phases using transmission electron microscopy (TEM) and energy dispersive x-ray spectroscopy (EDS). Determining the corrosion products formed on SS-15Zr alloy phases is critical to delineating the mechanisms of radionuclide release from the metal waste form.

EXPERIMENTAL

Specimens of SS-15Zr alloy, crushed to 75 to 150 μm size fraction, were immersed in 90°C deionized water for two years. The solution volume was such that the sample surface area-to-leachant volume ratio was ~2000 m^{-1}. On completion of the test, individual particles of the stainless steel and intermetallic phases were selected on the basis of scanning electron microscopy (SEM), embedded in resin, and sectioned by a Reichert-Jung Microtome to yield ~50-nm thick samples for TEM examination. Transmission electron microscopy was performed with a JEOL 2000FX unit operating at 200 kV and a PHILIPS CM30 unit operating at 300 kV, both equipped with an energy dispersive x-ray spectrometer. High-resolution TEM was carried out with a JEOL 4000EX microscope operating at 400 kV with a point-to-point resolution of 1.65 Å.

RESULTS AND DISCUSSION

Corrosion Products on an Austenite Particle

Figure 1 is a TEM image of corrosion products formed on an austenite particle from the reacted SS-15Zr alloy. The corrosion layer was largely detached from the metal, probably due to the mechanical force applied during ultramicrotomy. However, it was still possible to establish a spatial relationship between the metal surface and the corrosion layer. At least two distinct corrosion products formed on the surface. The corrosion product that appears to have been in immediate contact with the stainless steel surface (i.e., B in Fig. 1) exhibited a relatively dense and uniform microstructure, whereas the corrosion product on the outer surface of the layer (C in Fig. 1) was more porous. Assuming that no materials were lost during sample handling and preparation, the total layer thickness was estimated to be between 0.5 and 1.0 μm.

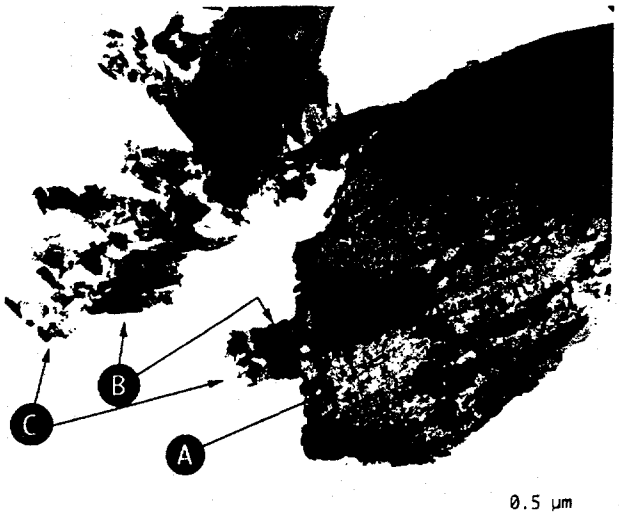

Figure 1. Bright-field TEM micrograph of an austenite–corrosion layer interface. At least two corrosion products (B and C) have formed on the stainless steel (A) surface, based on their distinctive microstructural characteristics.

Electron diffraction analyses indicated that both corrosion products were crystalline. The corrosion product B was indexed to match the cubic trevorite structure (JCPDS-ICDD 10-325, nominal formula $NiFe_2O_4$); the outer product C was indexed to match the face-centered cubic maghemite-c structure (JCPDS-ICDD 39-1346, nominal formula Fe_2O_3). The $NiFe_2O_4$ spinel was observed by Nakayama et al. [4, 5] in the passive film of 18Cr-8Ni austenitic stainless specimen that was heated in 300°C deoxygenated water for 24 h. This spinel structure was unaffected even after the sample was heated for 3 h at 1000°C. The presence of nickel in a spinel-type lattice was also reported by Castle and Clayton [6] in the oxide layer of a stainless steel alloy heated in 200°C water. These studies show that the spinel structure can be stabilized by nickel ions under appropriate experimental conditions.

Figure 2 compares the EDS spectra obtained from the austenite phase A, and the corrosion products B and C. The austenite spectrum has a minor zirconium peak, probably resulting from the small zirconium solubility in the phase. The corrosion product B consists mainly of Fe, Ni, and O, apparently consistent with the nominal composition of trevorite; $NiFe_2O_4$. The product C, which is part of the outer corrosion layer, appears to incorporate a small amount of Ni in the maghemite structure. Chromium was not observed in either corrosion product. This finding is somewhat surprising since the corrosion resistance of stainless steels is usually attributed to the presence of chromium in the passivation layer.

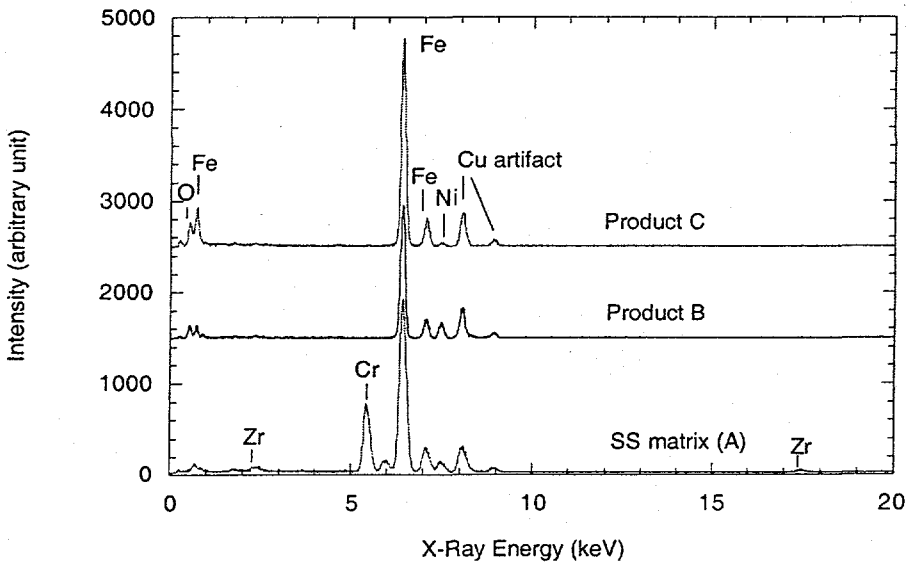

Figure 2. EDS spectra from the stainless steel (SS) matrix (austenite), and the corrosion products B and C. The corrosion products are enriched in Fe and Ni, and free of Cr.

Corrosion Products on an Intermetallic Particle

The corrosion layers formed on intermetallic particles were small and ranged in thickness from 10 to 100 nm. A bright-field TEM image of a typical corrosion layer is shown in Fig. 3; the layer is uniform and well adherent to the metallic surface. Electron diffraction patterns obtained from the intermetallic particle and corrosion layer are shown in Fig. 4a. The intermetallic was

identified as C15, the cubic Laves polytype. The corrosion layer exhibited broad diffuse rings (Fig. 4a), indicating that the layer was largely amorphous. The EDS analysis showed that the layer was enriched in Zr and Cr and depleted in Fe and Ni, when compared with the metallic matrix (Fig. 4b).

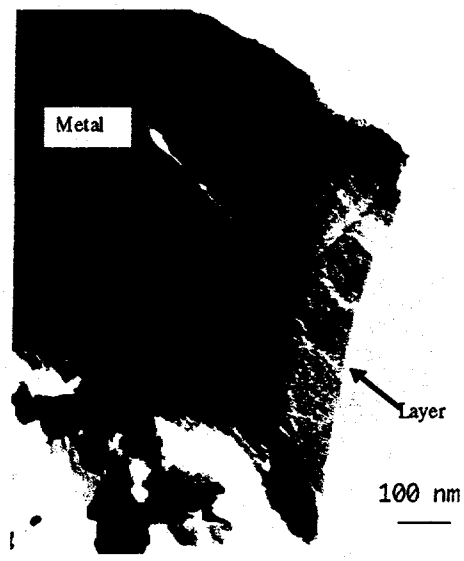

Figure 3. Bright-field TEM image of the corrosion layer formed on an intermetallic particle.

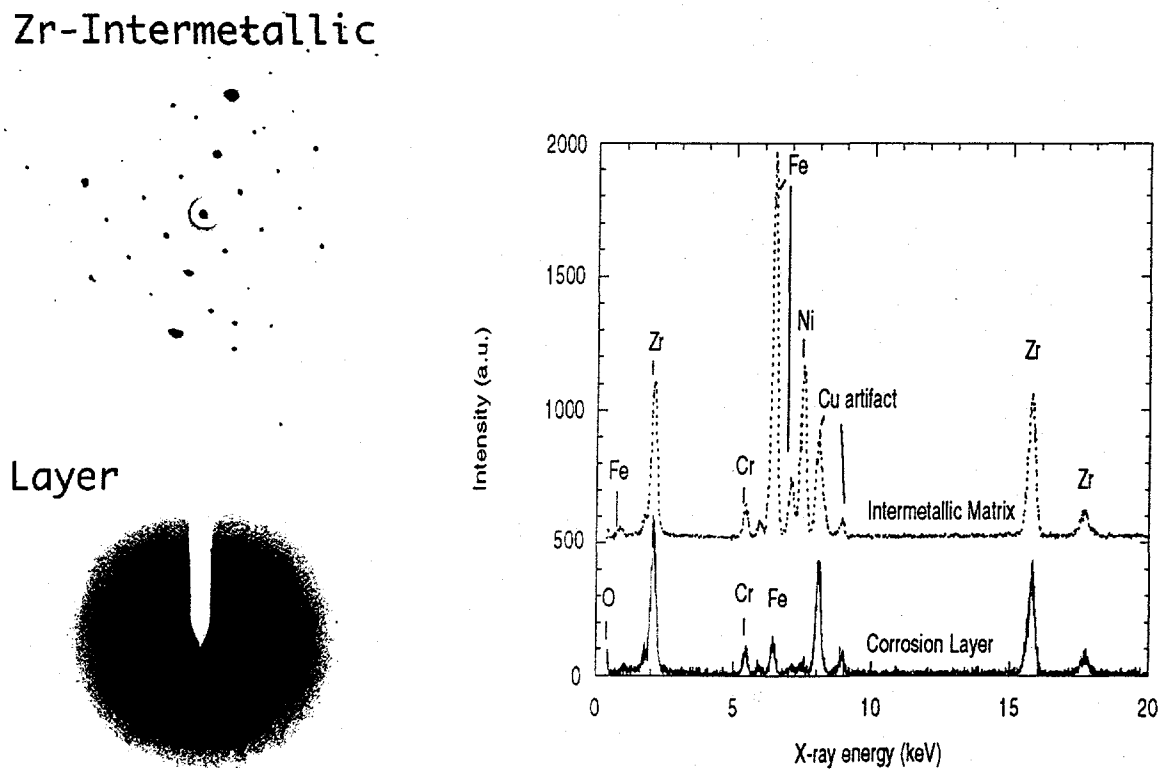

(A) (B)

Figure 4. Electron diffraction patterns (A) and EDS spectra (B) obtained from the intermetallic and the corrosion layer formed on its surface.

Figure 5 is a high-resolution TEM image of the intermetallic-corrosion layer interface. The crystalline intermetallic lattice was imaged along the [110] direction, and its (220) plane with a d-spacing of 0.25 nm was clearly resolved. The corrosion layer exhibited the typical contrast of a disordered lattice, which is consistent with the electron diffraction data. It is evident from Fig. 5 that the interface is not flat on the atomic scale. Domains of disorder are observed on the intermetallic side of the image, and small crystalline regions are detected in the amorphous corrosion layer. The interfacial configuration observed appears to be the result of a gradual transformation of the intermetallic into an amorphous corrosion product, probably due to the ingress of oxygen into the metal. Such an interlocking metal-oxide interface may explain the relatively strong adherence of the corrosion layer to the intermetallic surface.

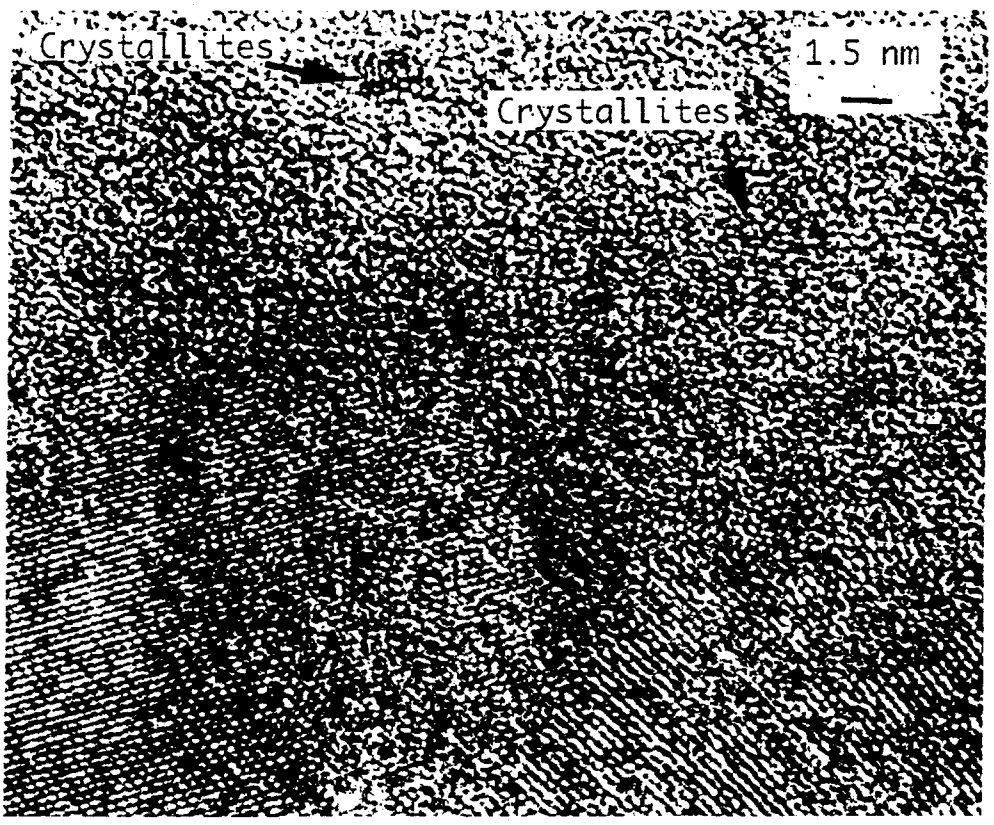

Figure 5. High-resolution TEM image of the intermetallic-corrosion layer interface. The image was taken along the [110] direction of C15, the cubic $ZrFe_2$ polytype. Crystallites observed in the amorphous corrosion layer (disordered zones) are shown by arrows.

The thinness of the corrosion layer indicates that the intermetallic is very resistant to corrosion. This may be because the corrosion layer is amorphous. Investigations in the Fe-Cr system have shown that alloy corrosion resistance increases with chromium content, with a dramatic improvement observed at ~12 wt% Cr [7, 8]. This result has been correlated to the increasing tendency of the oxide layer to become more disordered as the alloy chromium content increases, the suggestion being that an amorphous oxide is more resistant to breakdown than a crystalline oxide. Furthermore, amorphous oxides may be more protective because the mobility of ions may be smaller than in crystalline structures containing defects and grain boundaries [9]. In any case, the thin corrosion layers and the adherence of the layer to the intermetallic suggest

that fission products and actinide elements that are present in the oxide layer of the metal waste form could be retained on the alloy surface at least during the early stage of corrosion.

CONCLUSIONS

Corrosion layers formed on stainless steel–15Zr alloy particles that were reacted in 90°C deionized water for two years have been characterized. The corrosion products formed on an austenite particle were identified as trevorite ($NiFe_2O_4$) and maghemite-c (Fe_2O_3) with a small Ni content. Corrosion layers on intermetallic particles were uniform, adherent, amorphous, and enriched in Zr when compared with the intermetallic composition. High-resolution TEM images of the intermetallic-corrosion layer interface showed an interlocking metal-oxide, which suggests oxide formation due to oxygen ingress into the metal. The corrosion resistance of the intermetallic particles may be attributed to these amorphous oxide layers that effectively retard oxygen diffusion into the metal.

ACKNOWLEDGMENTS

This research was supported by the U.S. Department of Energy under Contract W-31-109-ENG-38. The authors thank R. Finch for assistance in sample preparation, and R. Cook and R. Csencsits for assistance in TEM operations.

REFERENCES

1. S.M. McDeavitt, D.P. Abraham, and J.Y. Park, J. Nucl. Mat. 257, 21-34 (1998).

2. D.P. Abraham, D.D. Keiser, Jr., and S.M. McDeavitt, Proc. Intl. Conf. on Decommissioning and Decontamination and on Nuclear and Hazardous Waste Management, Vol. 2, American Nuclear Society, LaGrange Park, IL p. 783 (1998).

3. D.P. Abraham, J.W. Richardson, Jr., and S.M. McDeavitt, Mat. Sci. Eng. A239-240, 658 (1997).

4. A. T. Nakayama and Y. Oshida, Corrosion 24, 336 (1968).

5. J. E. Castle and C. R. Clayton, Passivity of Metals, R. P. Frankenthal and J. Kruger, eds., The Electrochemical Society Inc, Princeton, NJ p.714 (1978).

5. G. Aronwitz and N. Hackerman, J. Electrochem. Soc. 110, 633 (1963).

6. C. L. McBee and J. Krueger, Electrochim. Acta 17, 1337 (1972).

9. T. P. Hoar, Palladium Medal Address, J. Electrochem. Soc. 117, 17c (1970).